Journal of The Electrochemical Society, **153** (5) G492-G497 (2006)
0013-4651/2006/153(5)/G492/6/$20.00 © The Electrochemical Society

High-Reliability Ta_2O_5 Metal–Insulator–Metal Capacitors with Cu-Based Electrodes

Kou-Chiang Tsai,[a] Wen-Fa Wu,[b,*,z] Chuen-Guang Chao,[a] and Cheng-Ping Kuan[b]

[a] *Department of Materials Science and Engineering, National Chiao Tung University, Hsinchu, Taiwan*
[b] *National Nano Device Laboratories, Hsinchu, Taiwan*

The properties of tantalum oxide (Ta_2O_5) metal–insulator–metal (MIM) capacitors with Al/Ta/Cu/Ta bottom electrodes were investigated. An ultrathin Al film successfully suppresses oxygen diffusion in the Ta_2O_5 MIM capacitor with the Cu-based electrode. The electrical characteristics and reliability of Ta_2O_5 MIM capacitors are improved by addition of ultrathin Al films. Ta_2O_5 MIM capacitors have low leakage current density (1 nA/cm^2 at 1 MV/cm) and high breakdown field (5.2 MV/cm at 10^{-6} A/cm^2). The decrease in leakage current is attributed to the formation of a dense and uniform Al_2O_3 layer, which has self-protection property and stops further oxygen diffusion into the tantalum contact. The dominant conduction mechanism of leakage current is the Poole–Frenkel effect at electric fields above 1.5 MV/cm.
© 2006 The Electrochemical Society. [DOI: 10.1149/1.2185283] All rights reserved.

Manuscript submitted March 10, 2005; revised manuscript received January 16, 2006. Available electronically March 27, 2006.

Metal–insulator–metal (MIM) capacitors are used as radio frequency (rf) capacitors in high-frequency circuits and analog capacitors in mixed-signal integrated circuit (IC) applications due to their high conductive electrodes and low parasitic capacitance.[1-3] As the circuit density increases, materials with a dielectric constant (ε) much higher than SiO_2 (~ 3.9) are desired.[4] Among various high-ε dielectric candidates, tantalum pentoxide (Ta_2O_5) has been studied as a promising material for a gate dielectric of metal-oxide semiconductor field effect transistors because of its high dielectric constant and excellent thermal and chemical stability.[5,6]

Current semiconductor technology demands the use of low-resistivity metals as electrode materials for ultralarge-scale integrated (ULSI) conduction lines and contact structures. In order to minimize the cost of ownership aspect in the electrode processes, several metallization technologies have been proposed in IC applications. Platinum (Pt) and ruthenium (Ru) have been used as the electrodes of capacitors with high-dielectric materials.[7,8] Pt and Ru, however, have limitations for application due to their high resistivity (Pt: $\sim$ 10.6 $\mu\Omega$ cm, Ru: $\sim$ 7.7 $\mu\Omega$ cm), cost, and leakage current.[9] Cu-based metallization technology could be incorporated into devices owing to ease of processing and reduction in production cost of silicon rf capacitors and mixed-signal ICs. In addition, Cu has low resistivity (1.67 $\mu\Omega$ cm) and high electro- and stress-migration resistance. However, Cu oxidizes during the initial stage of Ta_2O_5 reactive sputtering, and hillocks or particles are observed after annealing in oxygen ambient.[10,11] Significant efforts have been made to identify an appropriate diffusion barrier layer for Cu-based electrodes. Among these diffusion barrier materials, tantalum (Ta) is selected for Cu-based electrodes because it not only has low resistivity but also is thermodynamically stable with Cu.[12,13]

Unfortunately, the grain boundaries of a sputtered Ta layer generally provide paths for oxygen and copper diffusion when formation of Ta_2O_5 dielectrics requires processing under high temperature and oxygen ambient. Protection against oxidation and copper penetration is essential when growing Ta_2O_5 dielectric films on Cu-based electrodes. A capacitor structure using an ultrathin Al layer inserted between Ta_2O_5 dielectric and Ta diffusion barrier is proposed in this study. The improved characteristics of Ta_2O_5 MIM capacitors are investigated.

Experimental

Thermally grown SiO_2 films were formed on p-type Si(100) substrates for isolation. Three types of Cu-based bottom electrode layers were deposited by sputtering, (a) Cu (300 nm)/Ta (50 nm), (b) Ta (50 nm)/Cu (300 nm)/Ta (50 nm), and (c) Al (20 nm)/Ta (30 nm)/Cu (300 nm)/Ta (50 nm). The Ta film was deposited first and the Al film was the top layer for Al/Ta/Cu/Ta electrode layers. The Al/Ta/Cu/Ta electrode multilayers were formed by sequential sputtering of metal targets without breaking vacuum. Ta_2O_5 films of 40-nm thickness were deposited on Cu-based electrodes by reactive sputtering using a Ta target. During Ta_2O_5 deposition, Ar and O_2 mixture gases were introduced into the chamber to produce a total pressure of 3.5 mTorr. After Ta_2O_5 films were deposited, some wafers were postannealed at 500–600°C in oxygen ambient for 30 min. Then 50-nm Ta and 100-nm Cu films were deposited sequentially as top electrodes. Table I lists the MIM structures with multilayered bottom electrodes in the study.

The film thickness and refractive index were measured by field emission scanning electron microscopy (FESEM) and spectroreflectometry, respectively. The samples were investigated by cross-sectional transmission electron microscopy (XTEM) using a field emission microscope (JEOL JEM-2010F) and an acceleration voltage of 200 kV. The samples were prepared by mechanical grinding and polishing followed by ion milling under an acceleration voltage of 3–5 kV in a Gatan Duomill. Chemical reaction and oxygen penetration profile were characterized by secondary ion mass spectrometry (SIMS) and X-ray photoelectron spectrometry (XPS). Current-voltage (I-V) characteristics were used to investigate the leakage current and breakdown field. The breakdown field (E_{bd}) was defined as the electrical field when the current density through the dielectric exceeds 10^{-6} A/cm^2. To evaluate the reliability of the Ta_2O_5 film, time-dependent dielectric breakdown (TDDB) measurements using constant voltage stress were performed. Capacitors with an area of 3.14×10^{-4} cm^2 were employed.

Results and Discussion

Figure 1 illustrates SEM micrographs of the Ta_2O_5/Ta/Cu/Ta and Ta_2O_5/Al/Ta/Cu/Ta samples after annealing at 600°C in oxygen for 30 min. As displayed in Fig. 1a, the Ta_2O_5/Ta/Cu/Ta sample becomes rugged and forms particles and hillocks on the surface. Normally, oxygen easily penetrates the Ta layer via active diffusion paths and oxidizes the underlying layer. As shown in Fig. 1b, however, no hillocks are observed on the Ta_2O_5/Al/Ta/Cu/Ta sample surface. This indicates that Al/Ta barrier is impermeable to oxygen diffusion and protects the Cu layer underneath from oxidation.

Figure 2a illustrates the SIMS depth profiles of the O elements in the Ta_2O_5/Ta/Cu/Ta sample following annealing at 500 and 600°C in oxygen ambient. The annealing was performed after the Ta_2O_5 film was deposited. Oxygen diffusion is found after annealing. The oxygen contents in Ta and Cu films increase with increasing annealing temperature. Oxygen atoms diffuse along the grain boundaries of the Ta crystal and react with the Ta layer during annealing. The

* Electrochemical Society Active Member.
z E-mail: wfwu@mail.ndl.org.tw

Downloaded on 2014-04-26 to IP 140.113.38.11 address. Redistribution subject to ECS terms of use (see ecsdl.org/site/terms_use) unless CC License in place (see abstract).

Table I. MIM capacitors with various multilayered bottom electrodes used in the study.

Sample	Top electrode (nm)	Insulator (nm)	Bottom electrode (nm)
(a)	Cu (100)/Ta (50)	Ta_2O_5 (40)	Cu (300)/Ta (50)
(b)	Cu (100)/Ta (50)	Ta_2O_5 (40)	Ta (50)/Cu (300)/Ta (50)
(c)	Cu (100)/Ta (50)	Ta_2O_5 (40)	Al (20)/Ta (30)/Cu (300)/ Ta (50)

HRTEM image in Fig. 2b clearly shows that an interlayer of 4–5 nm thickness is formed between Cu and Ta layers after annealing at 600°C in oxygen. Figure 3a displays the SIMS depth profiles of the O elements in the Ta_2O_5/Al/Ta/Cu/Ta sample after annealing at 500 and 600°C. Almost no indication exists that oxygen atoms diffuse into the Ta and Cu layer. The SIMS observation shown is consistent with the HRTEM micrograph of Ta_2O_5/Al/Ta/Cu/Ta structures (Fig. 3b) after annealing at 600°C in oxygen. No oxygen defection or reaction is observed between the Ta and Cu layers in the Ta_2O_5/Al/Ta/Cu/Ta samples. Significant improvement in thermal stability is obtained, compared with the samples without thin Al film, apparently due to the barrier effectiveness of Al/Ta layers. However, the effective dielectric constant is about 18 instead of the value of 25 for pure Ta_2O_5. Figure 4 shows the TEM micrograph of the Cu/Ta/Ta_2O_5/Al/Ta/Cu device after thermal annealing at 600°C and reveals that the ultrathin film with an amorphous structure is formed between Ta_2O_5 and Al layers.

To identify this amorphous layer, the O 1s XPS spectra of Ta_2O_5 films deposited on Ta/Cu/Ta and Al/Ta/Cu/Ta electrodes were analyzed and are depicted in Fig. 5. Ta_2O_5 films were sputtered onto the electrodes for 5 min to form a layer of Ta_2O_5 of thickness $\leqslant$10-nm and then both samples were ion-etched in order to expose the interfaces of the Ta_2O_5–Ta and Ta_2O_5–Al. The O 1s spectra presented in Fig. 5a show that the oxygen photoelectrons are in the Ta–O state. The standard O 1s peak position is located at ~531 eV. The O 1s spectra presented in Fig. 5b show that the oxygen photoelectrons are in the Ta–O and Al–O states, indicating formation of an Al_2O_3layer.[14] In fact, formation of a dense monolayer of Al_2O_3 layer results in self-protection to oxidation and stops further oxygen diffusion. The layer behaves as an effective diffusion barrier to protect the underlying Cu and Ta layers.[15,16] The formation of Al_2O_3 is thermodynamically favorable compared to Cu oxide due to the large difference in oxide formation energy between Al (−226 kcal/g mol

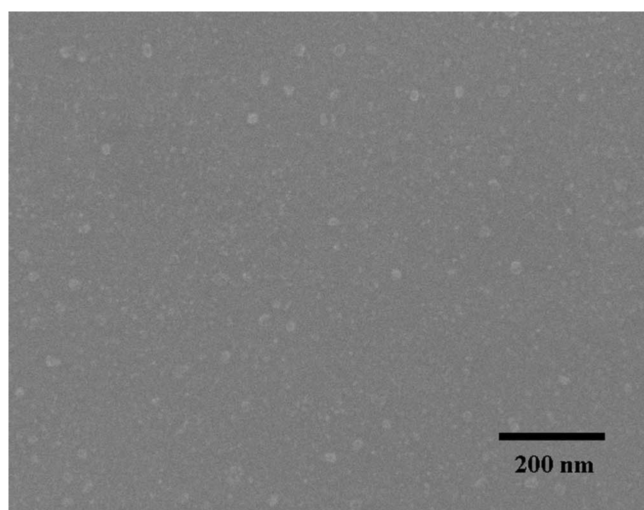

(a)

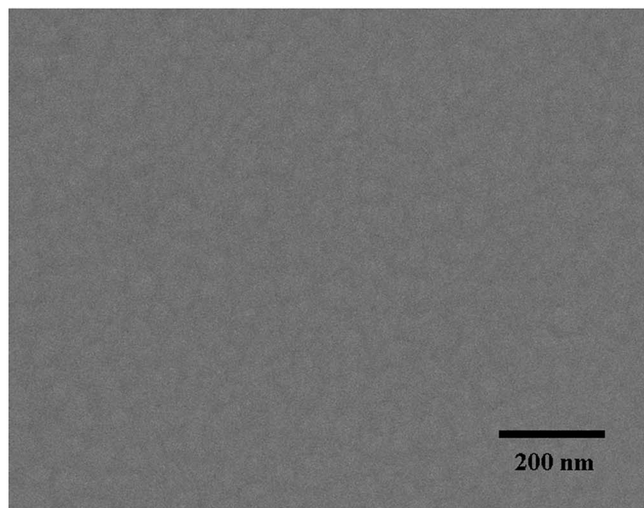

(b)

Figure 1. SEM images of the Ta_2O_5 films on (a) Ta/Cu/Ta and (b) Al/Ta/Cu/Ta bottom electrodes after annealing at 600°C for 30 min in oxygen ambient.

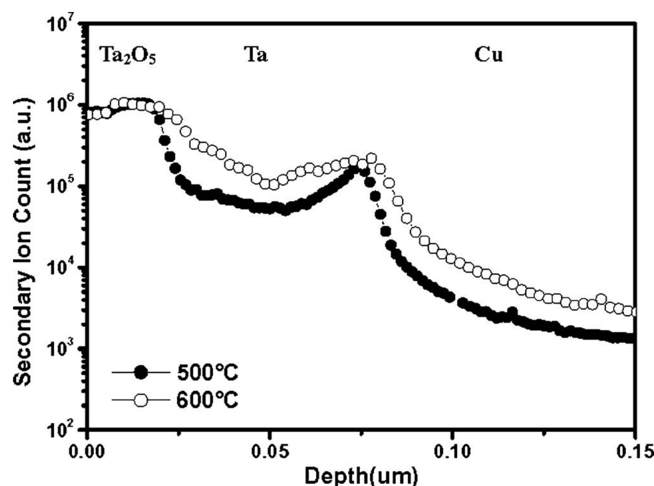

(a)

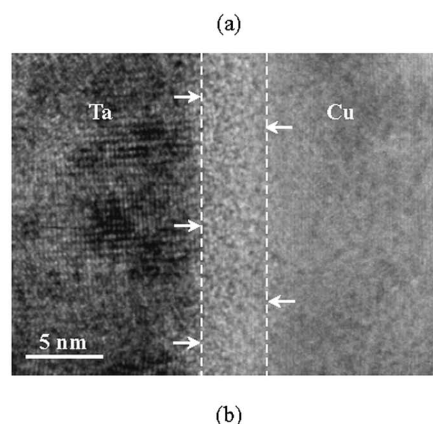

(b)

Figure 2. (a) SIMS depth profiles of O elements in the Ta_2O_5/Ta/Cu/Ta samples after furnace annealing at 500 and 600°C for 30 min in oxygen ambient. (b) HRTEM image of the interlayer between Ta and Cu layers in the Ta_2O_5/Ta/Cu/Ta sample.

Downloaded on 2014-04-26 to IP 140.113.38.11 address. Redistribution subject to ECS terms of use (see ecsdl.org/site/terms_use) unless CC License in place (see abstract).

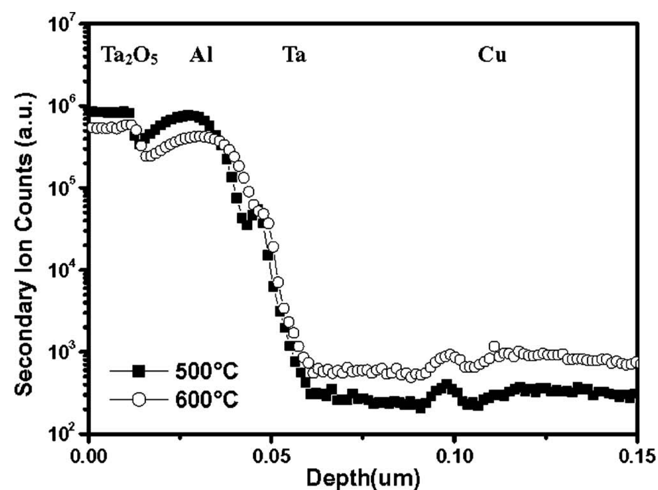

(a)

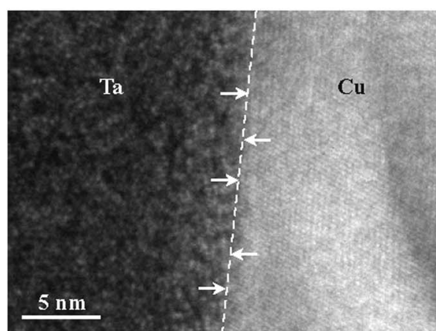

(b)

Figure 3. (a) SIMS depth profiles of O elements in Ta_2O_5/Al/Ta/Cu samples after furnace annealing at 500 and 600°C for 30 min in oxygen ambient. (b) HRTEM image of the region between Ta and Cu layers in the Ta_2O_5/Al/Ta/Cu/Ta sample.

O_2) and Cu (−53 kcal/g mol O_2). Therefore, the Al_2O_3 layer will behave as an effective diffusion barrier to protect the underlying Cu and Ta layers.

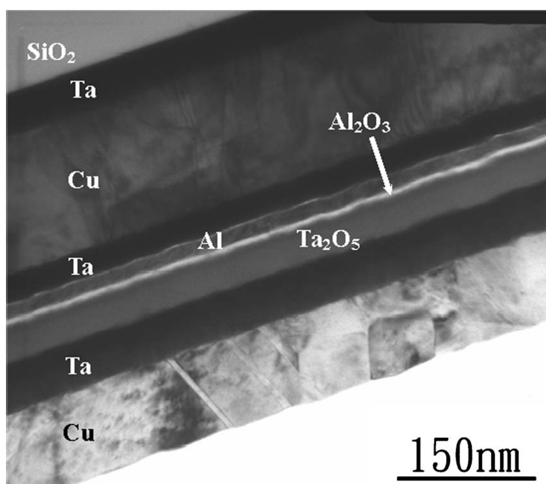

Figure 4. TEM image of the Cu/Ta/Ta_2O_5/Al/Ta/Cu/Ta MIM capacitor. The annealing was conducted at 600°C for 30 min in oxygen ambient after Ta_2O_5 film was deposited.

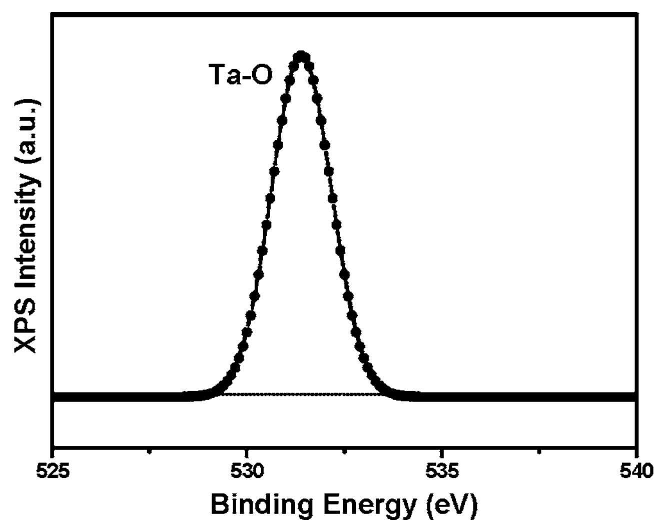

(a)

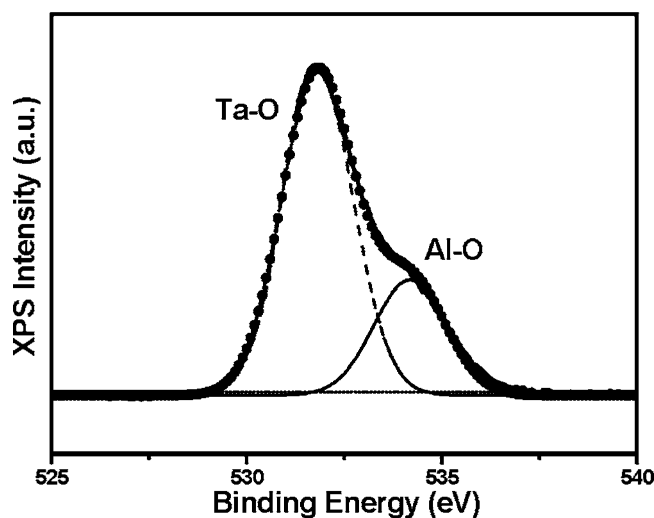

(b)

Figure 5. O 1s XPS spectra obtained from (a) Ta_2O_5–Ta interface for the Ta_2O_5/Ta/Cu/Ta sample and (b) Ta_2O_5–Al interface for the Ta_2O_5/Al/Ta/Cu/Ta sample.

Figure 6 displays leakage current densities of Ta_2O_5 films deposited on Al/Ta/Cu/Ta bottom electrodes after annealing at various temperatures in O_2 ambient. The thickness of the dielectric layer is the total thickness of the Ta_2O_5 and Al_2O_3 films. The leakage current density of the as-deposited Ta_2O_5 film is ~100 nA/cm^2 and decreases to ~1 nA/cm^2 at 1 MV/cm after annealing at 600°C due to elimination of oxygen vacancies and bond defects. Atanassova et al. have reported that oxygen annealing may affect the concentration of the oxygen vacancies and nonperfect bonds in the initial layers and consequently leads to leakage current reduction.[17] Several post-deposition treatments were investigated and successfully applied to reduce the oxygen vacancies and improve the electrical properties of Ta_2O_5 thin film.[6] Electrical properties of Ta_2O_5 MIM capacitors with various bottom electrodes, including Cu/Ta, Ta/Cu/Ta, and Al/Ta/Cu/Ta, were further compared and investigated. Figure 7 displays the leakage current densities as a function of electrical field up to 6 MV/cm following annealing at 600°C for 30 min. The leakage current densities are ~250 and 1.2–1.5 nA/cm^2 at 1 MV/cm for Cu/Ta and Ta/Cu/Ta bottom electrodes. The lowest leakage current density of 1 nA/cm^2 is measured for the Al/Ta/Cu/Ta bottom elec-

Downloaded on 2014-04-26 to IP 140.113.38.11 address. Redistribution subject to ECS terms of use (see ecsdl.org/site/terms_use) unless CC License in place (see abstract).

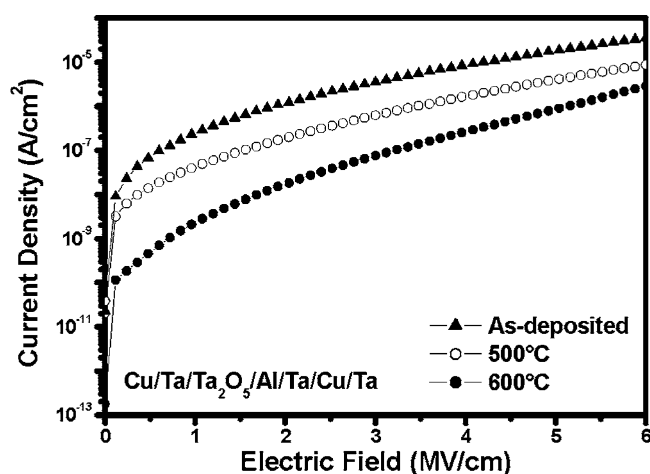

Figure 6. J-E characteristics of the Cu/Ta/Ta_2O_5/Al/Ta/Cu/Ta MIM capacitors after annealing at various temperatures in oxygen ambient for 30 min.

trode. Also, the leakage current densities of Ta_2O_5 MIM capacitors with Al/Ta/Cu/Ta bottom electrodes are much lower than those reported by Ezhivalavan and Tseng.[10,18] The breakdown field (E_{bd}) for the Al/Ta/Cu/Ta bottom electrode is approximately 5.2 MV/cm (at 10^{-6} A/cm^2) and higher than those for the Cu/Ta and Ta/Cu/Ta bottom electrodes of around 1.4 and 3.7 MV/cm.

Leakage current is a key parameter for ULSI circuit applications. The leakage current in the Ta_2O_5 MIM capacitor may be due to several mechanisms, including Schottky emission, Poole–Frenkel effect, electronic-hopping conduction, and tunneling.[6,17,19,20] The leakage current density vs electric field (J-E) characteristics of the MIM capacitor using bottom and top electrodes of different work functions are highly asymmetric with the voltage polarity for the Schottky emission and symmetric for the Poole–Frenkel emission.[21] In this study, symmetric J-E characteristics were observed for Ta_2O_5 MIM capacitors with Al/Ta/Cu/Ta bottom electrodes and Ta/Cu top electrodes. This behavior indicates that Poole–Frenkel emission is the possible dominant conduction mechanism for leakage currents. The Poole–Frenkel effect predicts a field-dependent behavior of the form

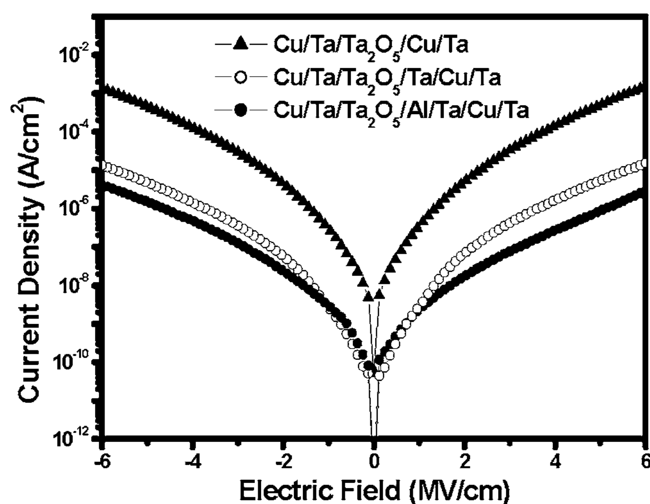

Figure 7. J-E characteristics of the Ta_2O_5 MIM capacitors with various bottom electrodes after annealing at 600°C in oxygen ambient for 30 min.

$$J = CE \exp\left(-\frac{q\phi_0}{kT}\right)\exp\left(\frac{\beta_{PF}}{kT}E^{1/2}\right) \quad [1]$$

where J denotes current density, T denotes the absolute temperature, q is the electronic charge, ϕ_0 is the barrier height, k represents the Boltzmann constant, E represents electric field, C is a constant, and β is defined by

$$\beta_{PF} = \left(\frac{q^3}{\pi\varepsilon_0\varepsilon}\right)^{1/2} \quad [2]$$

where ε_0 is the permittivity of free space and ε denotes the high-frequency dielectric constant. Poole–Frenkel conduction is due to field-enhanced thermal excitation of trapped electrons in the insulator into the conduction band. Figure 8a shows the logarithmic current density divided by the electric field as a function of the square root of the electric field [$\ln(J/E)$ vs $E^{1/2}$]. A good linearity is observed for the field $E > 1.5$ MV/cm for the plots. Furthermore, the dielectric constant deduced from the slope of the linear region of the Poole–Frenkel emission graph yields an ϵ value of 9.21, almost equal to that measured. The results indicate that the conduction mechanism is dominated by Poole–Frenkel effect for the field $E > 1.5$ MV/cm. In the case of the Al/Ta/Cu/Ta bottom electrode, the temperature dependence of J-E characteristics of the Ta_2O_5 capacitors was further studied. The leakage current increases exponentially with the temperature, as shown in Fig. 8b and c. These results reveal that it is affected by trap charge density, and the behavior shown in these plots indicates the Poole–Frenkel mechanism.

Figure 9a and b illustrates conduction mechanisms of Ta_2O_5 MIM capacitors with Ta/Cu/Ta and Al/Ta/Cu/Ta bottom electrodes. Some activated oxygen in the Ta_2O_5 film could diffuse into the Ta/Cu/Ta bottom electrode and react with the Ta layer during annealing. The oxygen vacancy acts as an electron trap with certain trap levels in the energy band diagram. The traps act as stepping sites for electrons and facilitate their transport through the oxide. Moreover, the barrier height becomes low when the oxygen vacancies accumulate at the interface of the Ta_2O_5–metal electrode.[22] Ta/Cu/Ta bottom electrodes could result in more oxygen vacancies at the Ta_2O_5–Ta interface compared to Al/Ta/Cu/Ta bottom electrodes. When the top electrode is positively biased, electrons are relatively easily injected from the Ta/Cu/Ta bottom electrode into the tantalum oxide layer and further conductivity is governed by Poole–Frenkel effect (Fig. 9a). An interfacial Al_2O_3 layer is formed at the Ta_2O_5–Al interface for the Al/Ta/Cu/Tabottom electrode. The formation of this layer can lead to modification of the conduction mechanism due to the difference in the bandgaps of Ta_2O_5 and Al_2O_3. Ta_2O_5 and Al_2O_3 have bandgaps of 4.4 and 8.8 eV, respectively.[23] It is found that the dominant conduction mechanism is also Poole–Frenkel effect for the Al/Ta/Cu/Ta bottom electrode from analyses of J-E characteristics. However, the interfacial Al_2O_3 layer will result in self-protection to oxidation and stop further oxygen diffusion. Reduction of oxygen vacancies leads to decreasing trap site, and leakage currents of Ta_2O_5 MIM capacitors with Al/Ta/Cu/Ta bottom electrodes could be reduced.

Nowadays, the TDDB is an important reliability indicator of the MIM capacitor. Figure 10 illustrates cumulative probabilities of breakdown fields for Ta_2O_5 MIM capacitors with various bottom electrodes. Breakdown is defined as occurring when the leakage current density increases to 10^{-6} A/cm^2. Obviously, the Cu/Ta/Ta_2O_5/Al/Ta/Cu/Ta MIM capacitors exhibit better breakdown behaviors than Cu/Ta/Ta_2O_5/Ta/Cu/Ta and Cu/Ta/Ta_2O_5/Cu/Ta MIM capacitors. Figure 11 shows the TDDB lifetime as a function of electric field for Ta_2O_5 MIM capacitors with various bottom electrodes. The Ta_2O_5 MIM capacitors with Al/Ta/Cu/Ta bottom electrodes have a longer lifetime than the others. The extrapolated long-term lifetime indicates that the Ta_2O_5 MIM capacitors with the Al/Ta/Cu/Ta bottom electrodes can survive 10 years at a stress field of 1.2 MV/cm. Moreover, the plotted points follow straight lines and random failure modes are not ob-

Downloaded on 2014-04-26 to IP 140.113.38.11 address. Redistribution subject to ECS terms of use (see ecsdl.org/site/terms_use) unless CC License in place (see abstract).

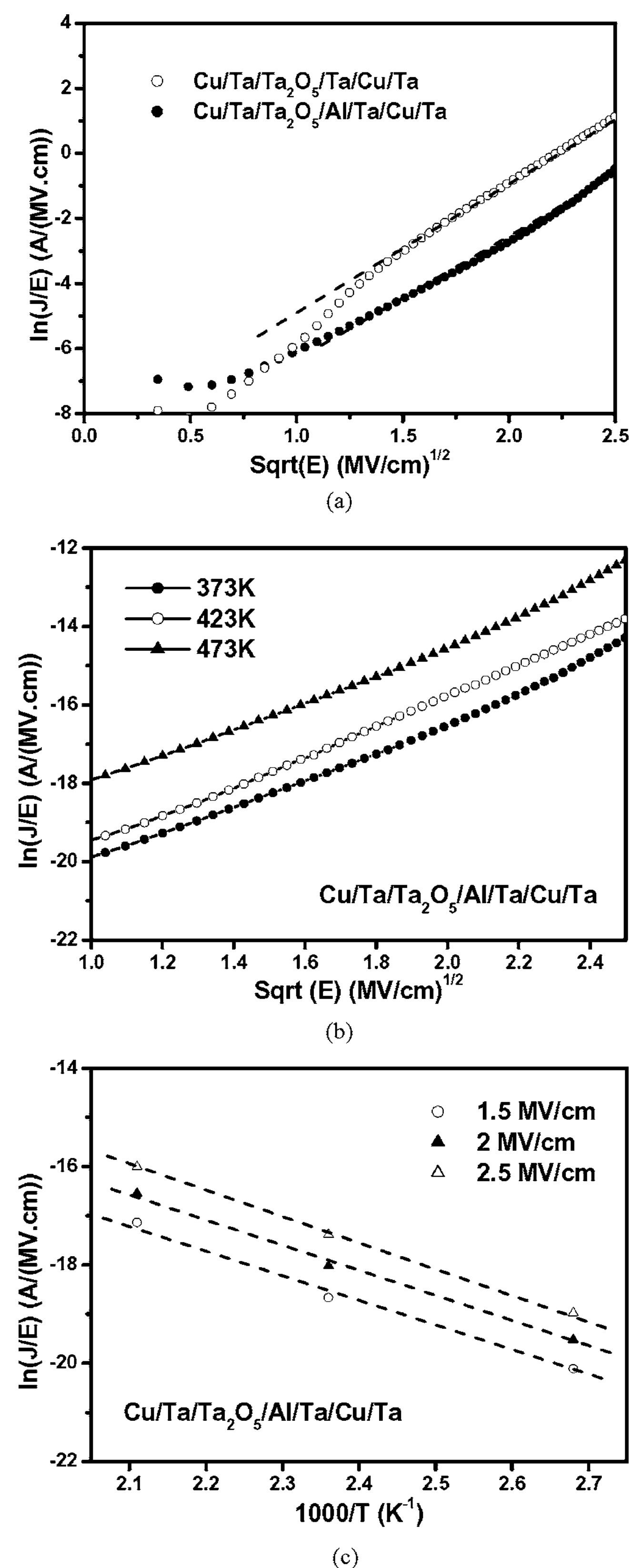

Figure 8. (a) $\ln(J/E)$ vs $E^{1/2}$ plots for the Ta_2O_5 MIM capacitors. (b) $\ln(J/E)$ vs $E^{1/2}$ plots for the Ta_2O_5 MIM capacitors with Al/Ta/Cu/Ta bottom electrodes at various measurement temperatures. (c) $\ln(J/E)$ vs $1000/T$ plots for the Ta_2O_5 MIM capacitors with Al/Ta/Cu/Ta bottom electrodes.

served, indicating the Ta_2O_5MIM capacitors with the Cu-based bottom electrodes are of high quality and good uniformity.

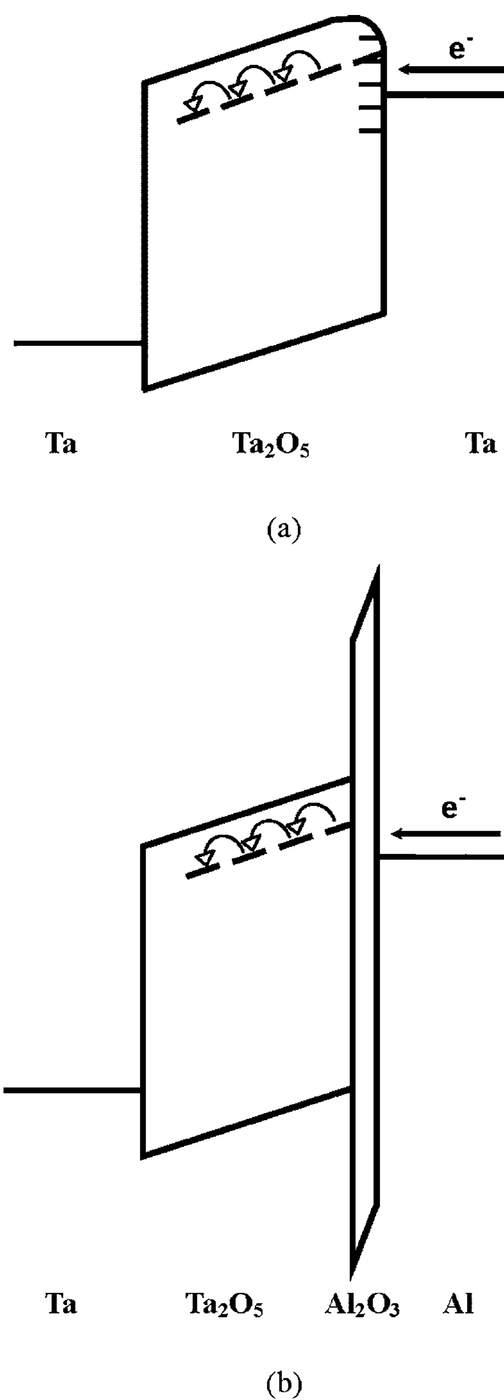

Figure 9. Schematic illustration of conduction mechanisms in Ta_2O_5 MIM capacitors with (a) Ta/Cu/Ta and (b) Al/Ta/Cu/Ta bottom electrodes biased at a positive voltage.

Conclusion

Multilayered Al/Ta/Cu/Ta electrodes enhance the properties of the Ta_2O_5 MIM capacitors with Cu-based electrodes. This work found that the capacitors demonstrated a significant improving capability against oxygen diffusion after inserting an Al film. This improvement is attributed to a dense Al_2O_3 film formed on the surface of the Al/Ta/Cu/Ta bottom electrode after thermal annealing in oxygen ambient. Ultralow leakage current density (1 nA/cm^2 at 1 MV/cm) and high breakdown field (5.2 MV/cm at 10^{-6} A/cm^2) are obtained for Ta_2O_5 MIM capacitors with Al/Ta/Cu/Ta electrodes because of reducing oxygen vacancy in tantalum oxide films.

Downloaded on 2014-04-26 to IP 140.113.38.11 address. Redistribution subject to ECS terms of use (see ecsdl.org/site/terms_use) unless CC License in place (see abstract).

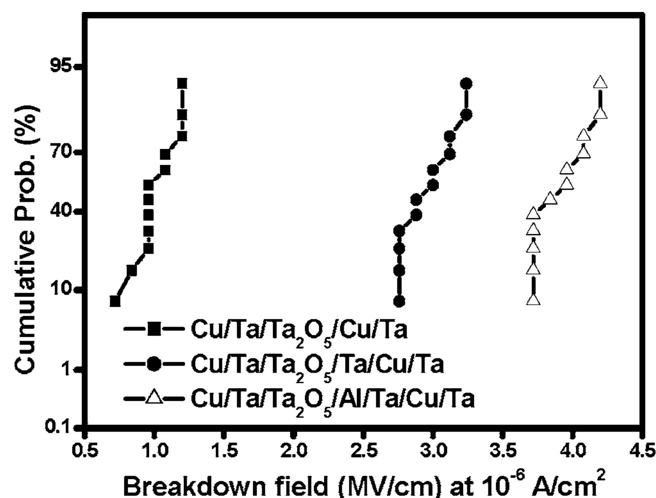

Figure 10. Cumulative probabilities of breakdown fields for Ta_2O_5 MIM capacitors with various bottom electrodes.

Ta_2O_5 MIM capacitors with Al/Ta/Cu/Ta electrodes also show less charge-trapping and better TDDB properties. Al/Ta/Cu/Ta electrodes enable the integration of Cu electrodes with high-dielectric-constant tantalum oxide thin films for high-frequency devices at interconnect levels.

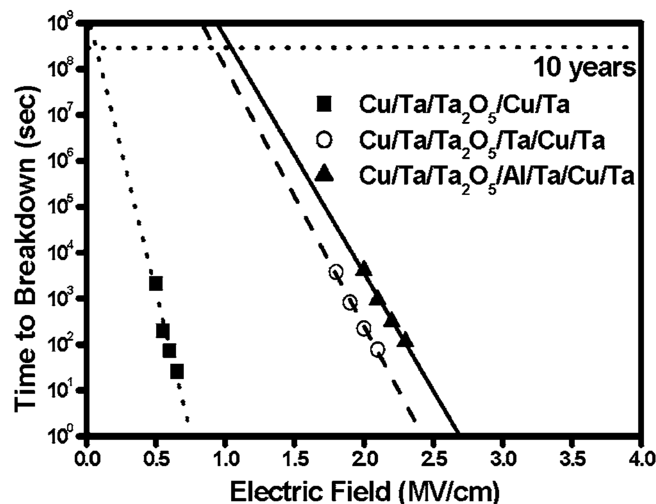

Figure 11. TDDB lifetime as a function of electric field for Ta_2O_5 MIM capacitors with various bottom electrodes.

Acknowledgments

The work was financially supported by the National Science Council of the Republic of China under contract no. NSC 94-2215-E-492-009 and supported, in part, by the Ministry of Economic Affairs of the Republic of China under contract no. 93-EC-17-A-08-S1-0003. Technical support from the National Nano Device Laboratories is gratefully acknowledged.

National Nano Device Laboratories assisted in meeting the publication costs of this article.

References

1. J. A. Babcock, S. G. Balster, A. Pinto, C. Dirnecker, P. Steinmann, R. Jumpertz, and B. El-Kareh, *IEEE Electron Device Lett.*, **22**, 230 (2001).
2. M. Armacost, A. Augustin, P. Felsner, Y. Feng, G. Friese, J. Heidenreich, G. Hueckel, O. Prigge, and K. Stein, *Tech. Dig. - Int. Electron Devices Meet.*, **2000**, 157.
3. A. Kar-Roy, C. Hu, M. Racanelli, C. A. Compton, P. Kempf, G. Jolly, P. N. Sherman, J. Zheng, Z. Zhang, and A. Yin, in *Proceedings of the IITC*, p. 245 (1999).
4. R. B. van Dover, R. M. Fleming, R. M. Schneemeyer, G. B. Alers, and D. J. Werder, *Tech. Dig. - Int. Electron Devices Meet.*, **1998**, 823.
5. W. D. Kim, J. H. Joo, Y. K. Jeong, S. J. Won, S. Y. Park, S. C. Lee, C. Y. Yoo, S. T. Kim, and J. T. Moon, *Tech. Dig. - Int. Electron Devices Meet.*, **2001**, 263.
6. C. Chaneliere, J. L. Autran, R. A. B. Devine, and B. Balland, *Mater. Sci. Eng., R*, **R22**, 269 (1998).
7. S. Ezhilvalavan and T. Y. Tseng, *J. Appl. Phys.*, **83**, 4797 (1998).
8. J. W. Lee, H. S. Song, K. M. Kim, J. M. Lee, and J. S. Roh, *J. Electrochem. Soc.*, **149**, F56 (2002).
9. J. H. Joo, J. M. Seon, Y. C. Jeon, K. Y. Oh, J. S. Roh, and J. J. Kim, *Appl. Phys. Lett.*, **70**, 3053 (1997).
10. S. Ezhilvalavan and T. Y. Tseng, *Thin Solid Films*, **360**, 268 (2000).
11. W. Fan, S. Saha, J. A. Carlisle, O. Auciello, R. P. H. Chang, and R. Ramesh, *Appl. Phys. Lett.*, **82**, 1452 (2003).
12. W. L. Yang, W. F. Wu, D. G. Liu, C. C. Wu, and K. L. Ou, *Solid-State Electron.*, **45**, 149 (2001).
13. W. F. Wu, K. L. Ou, C. P. Chou, and C. C. Wu, *J. Electrochem. Soc.*, **150**, G83 (2003).
14. J. F. Moulder, W. F. Stickle, P. E. Sobol, and K. D. Bomben, *Handbook of X-ray Photoelectron Spectroscopy*, p. 44 Physical Electronics, Eden Prairie, MN (1995).
15. W. A. Lanford, P. J. Ding, W. Wang, S. Hymes, and S. P. Muraka, *Thin Solid Films*, **262**, 234 (1995).
16. W. A. Lanford, S. Bedell, P. Isberg, B. Hjovarsson, S. K. Lakshmanan, and W. N. Gill, *J. Appl. Phys.*, **85**, 1487 (1999).
17. E. Atanassova, N. Novkovski, A. Paskaleva, and M. P. Gjorgjevich, *Solid-State Electron.*, **46**, 1887 (2002).
18. S. Ezhilvalavan and T. Y. Tseng, in *Proceedings of the Electronic Components and Technology Conference*, p. 1042 (1999).
19. S. M. Sze, *Physics of Semiconductor Device*, p. 478 Wiley, New York (1981).
20. C. Chaneliere, J. L. Autran, and R. A. B. Devine, *J. Appl. Phys.*, **86**, 480 (1999).
21. C. S. Chang, T. P. Liu, and T. B. Wu, *J. Appl. Phys.*, **88**, 7242 (2000).
22. J. H. Joo, Y. C. Jeon, J. M. Seon, K. Y. Oh, J. S. Roh, and J. J. Kim, *Jpn. J. Appl. Phys., Part 1*, **36**, 4382 (1997).
23. J. Robertson, *Appl. Surf. Sci.*, **190**, 2 (2002).

Downloaded on 2014-04-26 to IP 140.113.38.11 address. Redistribution subject to ECS terms of use (see ecsdl.org/site/terms_use) unless CC License in place (see abstract).